Atmos. Meas. Tech. Discuss., 5, 881–907, 2012
www.atmos-meas-tech-discuss.net/5/881/2012/
doi:10.5194/amtd-5-881-2012

Atmospheric Measurement Techniques Discussions

Multiple scattering in a dense aerosol atmosphere

S. Mukai[1], T. Yokomae[1], I. Sano[1], M. Nakata[1], and A. Kokhanovsky[2]

[1]Kinki University, 3-4-1 Kowakae, Higashi-Osaka, 577-8502, Japan
[2]University of Bremen, O. Hahn Allee 1, Bremen 28359, Germany

Received: 1 December 2011 – Accepted: 9 December 2011 – Published: 24 January 2012

Correspondence to: S. Mukai (mukai@info.kindai.ac.jp)

Published by Copernicus Publications on behalf of the European Geosciences Union.

Abstract

This study was designed to develop an efficient algorithm to retrieve aerosol characteristics in aerosol events, which are associated with dense concentrations of aerosols in the atmosphere, such as a dust storm or a biomass burning plume. The idea of successive scattering of light is reviewed based on the theory of radiative transfer. Then derivation of the method of successive order of scattering (MSOS) is interpreted in detail, and it is shown that MSOS is available for a simulation scheme in the dense radiation field being used to retrieve aerosol properties in the event with the high optical thickness. Finally our algorithms are practically applied for the biomass burning aerosol event over the Amazon using Aqua/MODIS data.

1 Introduction

This work is aimed at developing an efficient algorithm for retrieving aerosol characteristics in aerosol events such as dust storms and biomass burning plumes that are associated with excessive loading of aerosols in the atmosphere. It is also known that the dense soil dust that is transported from China to Japan on westerly winds, especially in spring, can have severe negative impacts on social life and human health. Furthermore, the increasing emissions of anthropogenic particles associated with continuing economic growth are increasing the concentrations of serious air pollutants. Thus it is well known that atmospheric aerosols are very complex and subject to heavy loading. Therefore, it is vital to be able to precisely retrieve aerosol characteristics. Our research group has been working on methods to retrieval aerosol characteristics based on the combined use of satellite data and ground measurements (Mukai, 1990; Sano et al., 2003), and numerical model simulations (Mukai et al., 2004).

It is known that the extreme concentrations of aerosols in the atmosphere during events such as dust storms and biomass burning plumes can prevent aerosol monitoring with surface-level sun/sky photometers, whereas satellites can still be used to observe the Earth's atmosphere from the space. This is why aerosol remote sensing

Discussion Paper | Discussion Paper | Discussion Paper | Discussion Paper |

AMTD

5, 881–907, 2012

Multiple scattering in a dense aerosol atmosphere

S. Mukai et al.

with satellites is well known to be useful and effective. Before attempting to retrieve aerosol properties from satellite data, the efficient algorithms for aerosol retrieval in the dense events need to be considered. Figure 1 shows a flow diagram for aerosol retrieval from satellite data. Our retrieval process is divided into three parts: satellite data analysis (S), model simulations (M) and radiative-transfer calculations (R). Aerosol properties such as the aerosol optical thickness (AOT), refractive index (m), and angstrom exponential (α) are estimated by comparing satellite measurements with the numerical values of radiation simulations in the Earth-atmosphere–surface model. The model of the Earth's atmosphere is based on the AFGL code, which provides the aerosol and molecule distributions with height (Kneizys et al., 1989). The multiple scattering calculations of radiative transfer take Rayleigh scattering by molecules and Mie scattering by aerosols in the atmosphere into account. The aerosol models are estimated from NASA/AERONET data (Holben et al., 1998; Dubovik et al., 2002; Omar et al., 2005).

Our satellite database includes various types of space-based measurements given by MODIS, GLI, CAI, ADEOS and so on. These space-borne sensors measure the upwelling radiance at the top of the atmosphere (TOA) from visible to far-infrared wavelengths. It is known that incident solar light interacts multiply with atmospheric aerosols, and hence simulating radiative transfer in the Earth's atmosphere represented by the box labeled "R.T. simulation" in Fig. 1 is a basic process for space-based aerosol retrieval. It is reasonable to consider that optical thickness of the atmosphere will increase during aerosol events, where incident solar radiation experiences multiple interactions with aerosols due to the dense radiation field. Namely, the precise simulation of multiple light-scattering processes needs a long computation time. Therefore, efficient algorithms are required for calculating the multiple scattering processes in an optically thick atmosphere model. The idea of successive scattering method (Uesugi et al., 1970), which is available for the radiation field reflected from the semi-infinite atmosphere, is interpreted in detail and applied for the aerosol events considered in the present study.

AMTD
5, 881–907, 2012

2 The successive scattering in the theory of radiative transfer

The idea of successive scattering is fundamentally related to the probabilistic approach to the theory of radiative transfer. Many papers have been written in this field and much progress has been made. However, since it is too heavy to review all of these here, only a narrow field which concerns directly to the successive scattering technique is simply reviewed in this section from the historical point of view.

2.1 The problem

The standard problem in the theory of radiative transfer is to get the reflection and, in case of finite medium, the transmission functions for a given medium with constant or depth-dependent albedo ϖ. The basic physical concept is simple. The intensity I is reduced by $e^{-d\tau}$ after traversing over an optical thickness $d\tau$ at a wavelength λ. The equation of transfer describes this circumstance as (Chandrasekhar, 1960)

$$\mu \frac{dI}{d\tau} = I - \frac{\varpi}{4\pi} \int P(\Omega, \Omega') I(\tau, \Omega') d\Omega', \tag{1}$$

where τ represents the optical thickness of atmosphere, ϖ is the albedo for single scattering, and $P(\Omega, \Omega')$ represents the phase function for single scattering, where μ is the cosine of the angle between the direction of light and outward normal of the medium. The boundary conditions for the standard problem are (i) at the top of the medium, $\tau = 0$, there are no radiation falling except in direction $-\mu_0$, and (ii) at the bottom of the medium, $\tau = \tau_0$, for the finite medium, no radiation incident on the medium at all, or, for the semi-infinite case.

Equation (1) with the boundary conditions above can be rewritten in terms of source function J,

$$J = \frac{\varpi}{4\pi} \int P(\Omega, \Omega') I(\tau, \Omega') d\Omega', \tag{2}$$

AMTD
5, 881–907, 2012

as

$$J(\tau) = \varpi \Lambda_r \{J(\tau)\} + e^{-\tau/\mu_0}, \tag{3}$$

where Λ denote the usual Λ-operator for semi-infinite or finite medium (Busbridge, 1960, chaps. 6 and 7) . The physical meaning of this equation is not unclear. The term $e^{-\tau/\mu_0}$ corresponds to the probability of direct transmission over the distance τ in direction μ_0, and Λ the multiple scattering (Sobolev, 1963, chap. 6). The reflection and transmission functions are obtained through Laplace transform of J.

A more direct approach to the problem is to formulate a set of functional equations for the reflection and transmission functions. The principle of invariance stated originally by Ambartsumian and examined extensively by Chandrasekhar is elegant to attack the problem. The integral equation for the reflection function R in case of semi-infinite medium which is related to H-function is given by Chandrasekhar (1960, chap. IV). And, in case of finite medium, the reflection and transmission functions are related to X and Y function and the equations for them are given also by Chandrasekhar (1960, chap. VII).

2.2 Successive approximation

Equation (3) suggests an iterative solution of a form (Sobolev, 1963, chap. 2, Sect. 1).

$$J_n(\tau) = \Lambda J_{n-1}(\tau), n \geq 1 \tag{4}$$

$$J_0(\tau) = e^{-\tau/\mu_o} \tag{5}$$

and

$$J(\tau) = \sum_{n=0}^{\infty} \varpi^n J_n(\tau) \tag{6}$$

This is nothing other than to expand $J(\tau)$ in terms of ϖ^n, that is, Neumann series solution. The physical meaning of these equations is obvious. Equation (5) gives the

AMTD
5, 881–907, 2012

Discussion Paper | Discussion Paper | Discussion Paper | Discussion Paper |
Title Page
Abstract Introduction
Conclusions References
Tables Figures
◀◀ ▶▶
◀ ▶
Back Close
Full Screen / Esc
Printer-friendly Version
Interactive Discussion

source function which is composed of photons scattered only once, and Eq. (4) for photons "processed" twice or more. The entire source function (Eq. 6) is a weighted sum of these source functions by ϖ^n, since a photon survives with probability ϖ at a single act of scattering.

It is easy to treat Eq. (6) with only first two or three terms (Hulst, van de 1949) though, the numerical computation must be consulted beyond the 3rd order. The direct treatment on the reflection and transmission functions in this respect is also possible. We can derive a set of recurrence relation between the n-th order function add the lower ones from some mathematical manipulation starting from Eq. (6) or from some physical reasoning (Uesugi et al., 1970). The problem in this successive approximation method is the slowness of the convergence in Eq. (3). When ϖ is small compared to one, or when the thickness of the medium is small, the computation is easy. However, when $\varpi \rightarrow$ x and medium becomes semi-infinite, the labour is formidable.

2.3 Refined technique

To overcome the difficulty, an important progress was made by van de Hulst (Hulst, van de 1963). For a finite medium, the n-th order source function J_n is practically equal to ηJ_{n-1} where η is the largest eigen value of the integral equation

$$\eta J = \Lambda\{J\}. \tag{7}$$

Hence, when n is sufficiently large, we can regard the sum in Eq. (6) as a geometrical series, and the computation becomes simple. The eigen value η for isotropic scattering, which is a function of optical thickness τ_0 of the medium, is given in a tabular form by van de Hulst (Hulst, van de 1963). The value of η becomes unity when the thickness approaches to infinity. This means that the replacement of Eq. (6) by a geometrical series becomes unsafe when $\tau \rightarrow \infty$ and $\varpi \rightarrow 1$. So van de Hulst invoked another technique, the "doubling method". This technique has been used in the planetary atmosphere model and provided to be useful (Hansen et al., 1974). It may be considered an extension of the idea of successive scattering.

The second technique to overcome the slow convergence of Eq. (6) is to express the higher order reflection function by an asymptotic form. The connection between this asymptotic form and the problem in nearly conservative thick atmosphere has been discussed, and it is found that the n-th order reflection function (R_n) at the TOA of a semi-infinite medium can be expressed as (Uesugi et al., 1970; Hulst, 1980, Kokhanovsky, 2002):

$$R_n \sim An^{-3/2}. \tag{8}$$

The variable A in the above equation is independent on albedo.

3 Method of Successive Order of Scattering (MSOS)

3.1 Successive order of scattering for a semi-infinite model

It seems not trivial to examine if the successive scattering technique mentioned in the previous section is useful to the radiation field reflected from the optically semi-infinite atmosphere model, which is available for our present problem of aerosol events. Suppose there is an incident radiation of flux F in direction (μ_0, ϕ_0) falling on the top of a semi-infinite atmosphere. So the emergent intensity I_{em} is given by using total reflection R

$$I_{em} = \frac{1}{\mu}\frac{1}{4\pi}\int_{-}^{RF\,d\Omega'}, \tag{9}$$

where the integration covers inward hemisphere. Also we can define the n-th order reflection in Eq. (8) as:

$$R(\Omega, \Omega_0) = \sum_{n=1}^{\infty} \varpi^n R(n:\Omega, \Omega_0), \tag{10}$$

AMTD
5, 881–907, 2012

where n is the number of scatterings and $R(n:\Omega,\Omega_0)$ is the nth-order reflection function, which describes the radiation emerging at the TOA after scattering n times within the atmosphere.

The equation for the n-th order of reflection will be derived here as follows. Let the diffusely reflected radiation intensity be I. Decomposing I into the successively scattered intensity $I(n)$, i.e.,

$$I = \sum_{n=1}^{\infty} \varpi^n I(n). \tag{11}$$

We have a defining equation for $R(1)$ as

$$I(1) = \frac{1}{\mu}\frac{1}{4\pi}\int_{-} R(1) F\, d\Omega, \tag{12}$$

where the integration is over inward half space. Now, when a layer of thickness Δ is added at the TOA of this semi-infinite medium, the radiation field becomes

$$\begin{aligned} I(1:\Omega,\Delta) = {} & \tfrac{1}{\mu}\tfrac{1}{4\pi}\textstyle\int_{-} d\Omega' \,\Delta\, P(\Omega,\Omega')F(\Omega') \\ & + \tfrac{1}{\mu}\tfrac{1}{4\pi}\textstyle\int_{-} \left(1-\tfrac{\Delta}{\mu}\right) R(1:\Omega,\Omega')\left(1-\tfrac{\Delta}{\mu'}\right) F(\Omega')\, d\Omega', \end{aligned}$$

or

$$\begin{aligned} I(1:\Omega,\Delta) = {} & \tfrac{1}{\mu}\tfrac{\Delta}{4\pi}\textstyle\int_{-} P(\Omega,\Omega')F(\Omega')\, d\Omega' \\ & - \tfrac{1}{\mu}\tfrac{\Delta}{4\pi}\textstyle\int_{-} \left(\tfrac{1}{\mu}+\tfrac{1}{\mu'}\right) R(1:\Omega,\Omega')F(\Omega')\, d\Omega' \\ & + \tfrac{1}{\mu}\tfrac{1}{4\pi}\textstyle\int_{-} R(1:\Omega,\Omega')F(\Omega')\, d\Omega'. \end{aligned} \tag{13}$$

Since $I(1, \Delta)$ must be equal to $I(1)$, we get

$$\int_{-} \left(\frac{1}{\mu}+\frac{1}{\mu'}\right) R(1:\Omega,\Omega')F(\Omega')\, d\Omega' = \int_{-} P(\Omega,\Omega')F(\Omega')\, d\Omega'. \tag{14}$$

Now, letting

$$F(\Omega') = \delta(\mu'-\mu_0)\,\delta(\phi'-\phi_0)\,E, \tag{15}$$

AMTD

5, 881–907, 2012

Title Page
Abstract | Introduction
Conclusions | References
Tables | Figures
◂◂ | ▸▸
◂ | ▸
Back | Close
Full Screen / Esc
Printer-friendly Version
Interactive Discussion

where E is unity, we obtain

$$\left(\frac{1}{\mu}+\frac{1}{\mu_0}\right)R(1:\Omega,\Omega_0)=P(\Omega,\Omega_0). \tag{16}$$

For the second order one, we have a defining equation as

$$I(2,\Omega)=\frac{1}{\mu}\frac{1}{4\pi}\int_{-}R(2:\Omega,\Omega')F(\Omega')d\Omega', \tag{17}$$

and with the same reasoning as above, we get

$$\begin{aligned}I(2:\Omega,\Delta)=&\int_{-}^{\frac{1}{4\pi}\int_{-}\frac{1}{4\pi}\left(1-\frac{\Delta}{\mu}\right)\frac{1}{\mu}R(1:\Omega,\Omega')\frac{\Delta}{\mu'}P(\Omega',\Omega'')F(\Omega'')d\Omega'd\Omega''}\\&+\int_{-}^{\frac{1}{4\pi}\int_{-}\frac{1}{4\pi}\frac{\Delta}{\mu}P(\Omega,\Omega')\frac{1}{\mu'}R(1:\Omega',\Omega'')\left(1-\frac{\Delta}{\mu''}\right)F(\Omega'')d\Omega'd\Omega''}\\&+\int_{-}^{\frac{1}{4\pi}\left(1-\frac{\Delta}{\mu}\right)\frac{1}{\mu}R(2:\Omega,\Omega'')\left(1-\frac{\Delta}{\mu''}\right)F(\Omega'')d\Omega''},\end{aligned}$$

or

$$\begin{aligned}I(2:\Omega,\Delta)=&\Delta\int_{-}^{\frac{1}{4\pi}\int_{+}\frac{1}{4\pi}\frac{1}{\mu}R(1:\Omega,\Omega')\frac{1}{\mu'}P(\Omega',\Omega'')F(\Omega'')d\Omega'd\Omega''}\\&+\Delta\int_{-}^{\frac{d}{4\pi}\int_{+}\frac{1}{4\pi}\frac{1}{\mu}P(\Omega,\Omega')\frac{1}{\mu'}R(1:\Omega',\Omega'')F(\Omega')d\Omega'd\Omega''}\\&-\Delta\int_{-}^{\frac{1}{4\pi}\left(\frac{\Delta}{\mu}+\frac{\Delta}{\mu''}\right)\frac{1}{\mu}R(2:\Omega,\Omega'')F(\Omega'')d\Omega''}\\&+\int_{-}^{\frac{1}{4\pi}\frac{1}{\mu}R(2:\Omega,\Omega'')F(\Omega'')d\Omega''}.\end{aligned} \tag{18}$$

Then, with Eq. (15), we have

$$\begin{aligned}\left(\frac{1}{\mu}+\frac{1}{\mu_0}\right)R(2:\Omega,\Omega_0)=&\int_{+}\frac{1}{4\pi}R(1:\Omega,\Omega')\frac{1}{\mu'}P(\Omega',\Omega_0)d\Omega'\\&+\int_{+}\frac{1}{4\pi}P(\Omega',\Omega_0)\frac{1}{\mu'}R(1:\Omega,\Omega')d\Omega'.\end{aligned} \tag{19}$$

Generally, the equation for the n-th order $R(\mathrm{n})$ (n≥3) can be derived in a similar manner as above. Then the n-th order emergent intensity $I(n)$ is expressed as

$$I(n)=\frac{1}{\mu}\frac{1}{4\pi}\int_{-}R(n:\Omega,\Omega')F(\Omega')d\Omega'. \tag{20}$$

AMTD
5, 881–907, 2012

And also

$$
\begin{aligned}
I(n:\Omega,\Delta) = {} & \int_{-} \frac{1}{4\pi}\int_{-}\frac{1}{4\pi}\left(1-\frac{\Delta}{\mu}\right)\frac{1}{\mu}R(n-1:\Omega,\Omega')\frac{\Delta}{\mu'}P(\Omega',\Omega'')F(\Omega'')\,d\Omega''\,d\Omega' \\
& + \int_{+} \frac{1}{4\pi}\int_{-}\frac{1}{4\pi}\frac{\Delta}{\mu}P(\Omega,\Omega')\frac{1}{\mu'}R(n-1:\Omega',\Omega'')\cdot\left(1-\frac{\Delta}{\mu''}\right)F(\Omega'')\,d\Omega'' \\
& + \sum_{n'=1}^{n-2}\int_{-}\frac{1}{4\pi}\int_{+}\frac{1}{4\pi}\int_{-}\frac{1}{4\pi}\left(1-\frac{\Delta}{\mu}\right)R(n':\Omega,\Omega')\,\frac{\Delta}{\mu'}P(\Omega',\Omega'') \\
& \qquad \times \frac{\Delta}{\mu''}P(\Omega'',\Omega''')\left(1-\frac{\Delta}{\mu'''}\right)F(\Omega''')\,d\Omega'''\,d\Omega''\,d\Omega' \\
& + \int_{-}\frac{1}{4\pi}\left(1-\frac{\Delta}{\mu}\right)\frac{1}{\mu}R(n:\Omega,\Omega''')\left(1-\frac{\Delta}{\mu'''}\right)F(\Omega''')\,d\Omega''' .
\end{aligned}
\tag{21}
$$

Hence

$$
\begin{aligned}
\left(\frac{1}{\mu}+\frac{1}{\mu_0}\right)R(n:\Omega,\Omega'')
& = \int_{-}\frac{1}{4\pi}R(n-1:\Omega,\Omega')\frac{1}{\mu'}P(\Omega',\Omega_0)\,d\Omega' \\
& + \int_{+}\frac{1}{4\pi}P(\Omega,\Omega')\frac{1}{\mu'}R(n-1:\Omega,\Omega_0)\,d\Omega' \\
& + \sum_{n'=1}^{n-1}\int_{-}\frac{1}{4\pi}\int_{+}\frac{1}{4\pi}R(n':\Omega,\Omega')\frac{1}{\mu'}P(\Omega',\Omega'')\frac{1}{\mu''}R(n-n'-1:\Omega'',\Omega_0)\,d\Omega''\,d\Omega' .
\end{aligned}
\tag{22}
$$

Defining a new reflection function R^* as

$$\mu\mu_0 R^*(\Omega,\Omega_0) = R(\Omega,\Omega_0), \tag{23}$$

and writing R^* as R, we have

$$(\mu+\mu_0)R(1:\Omega,\Omega_0) = P(\Omega,\Omega_0), \tag{24}$$

$$(\mu+\mu_0)R(2:\Omega,\Omega_0) = \frac{\mu}{4\pi}\int_{-}R(1:\Omega,\Omega')P(\Omega',\Omega_0)\,d\Omega' + \frac{\mu_0}{4\pi}\int_{+}P(\Omega,\Omega')R(1:\Omega',\Omega_0)\,d\Omega', \tag{25}$$

AMTD
5, 881–907, 2012

$$
\begin{aligned}
(\mu+\mu_0)R(n:\Omega,\Omega_0) \\
&= \frac{\mu}{4\pi}\int_{-} R(n-1:\Omega,\Omega')P(\Omega',\Omega_0)d\Omega' \\
&+ \frac{\mu_0}{4\pi}\int_{+} P(\Omega',\Omega_0)R(n-1:\Omega',\Omega_0)d\Omega' \\
&+ \frac{\mu\mu_0}{(4\pi)^2}\sum_{n'=1}^{n-2}\int_{-}\int_{+} R(n':\Omega,\Omega')P(\Omega',\Omega'')R(n-n'-1:\Omega'',\Omega_0)d\Omega'' \, d\Omega',
\end{aligned}
\tag{26}
$$

Thus the radiation field reflected from the optically semi-infinite atmosphere is calculated based on Eq. (10) by utilizing Eqs. (24), (25) and (26). This technique is named MSOS (method of successive order of scattering).

3.2 Fourier expansion

The angles Ω and Ω' represent the propagation and incident directions, which are characterized by the zenith angle (θ) and the azimuth angle (ϕ). Note that the cosine of the zenith angel ($\mu = \cos\theta$p is usually used in stead of zenith angle itself. Thus, the scattering angle (Θ) for a single scattering process is expressed as

$$\cos\Theta = \mu\mu' + \sqrt{1-\mu^2}\sqrt{1-\mu'^2}\cos(\phi-\phi'). \tag{27}$$

Therefore, phase function $P(\Omega,\Omega_0)$ is written as $P(\mu,\mu_0,\phi-\phi_0)$, which can be expanded using Fourier series with respect to $\phi-\phi_0$ for the enable efficient calculations of multiple light scattering:

$$P(\Omega,\Omega_0) = P(\mu,\mu_0) + 2\sum_{l=1}^{\infty}[P_c^l(\mu,\mu_0)\cos l(\phi-\phi_0) + P_s^l(\mu,\mu_0)\sin l(\phi-\phi_0)]. \tag{28}$$

Similarly reflection function $R(n,\Omega,\Omega_0)$ is also expanded in the Fourier series as (Mukai et al., 1979):

$$R = R^0(n:\mu,\mu_0) + 2\sum_{l=1}^{\infty}\left[R_c^{(l)}(n:\mu,\mu_0)\cos l(\phi-\phi_0) + R_s^{(l)}(n:\mu,\mu_0)\sin l(\phi-\phi_0)\right]. \tag{29}$$

AMTD
5, 881–907, 2012

Title Page
Abstract | Introduction
Conclusions | References
Tables | Figures
◄ | ►
◄ | ►
Back | Close
Full Screen / Esc
Printer-friendly Version
Interactive Discussion

The equations for the Fourier coefficients corresponding to Eq. (29) are derived from Eq. (24)

$$(\mu+\mu_0)R^{(0)}(1:\mu,\mu_0)=P^{(0)}(\mu,\mu_0), \tag{30}$$

$$(\mu+\mu_0)R_c^{(l)}(1:\mu,\mu_0)=P_c^{(l)}(\mu,\mu_0), \quad l=1,2,\cdots \tag{31}$$

$$(\mu+\mu_0)R_s^{(l)}(1:\mu,\mu_0)=P_s^{(l)}(\mu,\mu_0), \quad l=1,2,\cdots \tag{32}$$

Similarly from Eq. (25),

$$\begin{aligned}(\mu+\mu_0)&R^{(0)}(2:\mu,\mu_0)\\ &=\frac{\mu}{2}\int_{-1}^{0}R^{(0)}(1:\mu,\mu')P^{(0)}(\mu',\mu_0)\,d\mu' \ ,\\ &+\frac{\mu_0}{2}\int_0^1 P^{(0)}(\mu,\mu')\cdot R^{(0)}(1:\mu',\mu_0)\,d\mu'\end{aligned} \tag{33}$$

$$\begin{aligned}(\mu+\mu_0)&R_c^{(l)}(2:\mu,\mu_0)\\ &=\frac{\mu}{2}\int_{-1}^{0}\left[R_c^{(l)}(1:\mu,\mu')P_c^{(l)}(\mu',\mu_0)-R_s^{(l)}(1:\mu,\mu')P_s^{(l)}(\mu',\mu_0)\right]d\mu' \ ,\\ &+\frac{\mu_0}{2}\int_0^1\left[P_c^{(l)}(\mu,\mu')R_c^{(l)}(1:\mu',\mu_0)-P_s^{(l)}(\mu,\mu')R_s^{(l)}(1:\mu',\mu_0)\right]d\mu'\\ &\qquad l=1,2,\cdots\end{aligned} \tag{34}$$

$$\begin{aligned}(\mu+\mu_0)&R_s^{(l)}(2:\mu,\mu_0)\\ &=\frac{\mu}{2}\int_{-1}^{0}\left[R_s^{(l)}(1:\mu,\mu')P_c^{(l)}(\mu',\mu_0)+R_c^{(l)}(1:\mu,\mu')P_s^{(l)}(\mu',\mu_0)\right]d\mu'\\ &+\frac{\mu_0}{2}\int_0^1\left[P_s^{(l)}(\mu,\mu')R_c^{(l)}(1:\mu',\mu_0)+P_c^{(l)}(\mu,\mu')R_s^{(l)}(1:\mu',\mu_0)\right]d\mu' .\\ &\qquad l=1,2,\cdots\end{aligned} \tag{35}$$

AMTD
5, 881–907, 2012

Title Page
Abstract | Introduction
Conclusions | References
Tables | Figures
◂ | ▸
Back | Close
Full Screen / Esc
Printer-friendly Version
Interactive Discussion

Equation (26) provides us with

$$
\begin{aligned}
&(\mu+\mu_0)R^{(0)}(n:\mu,\mu_0)\\
&\quad=\frac{\mu}{2}\int_{-1}^{0}R^{(0)}(n-1:\mu,\mu')P^{(0)}(\mu',\mu_0)\,d\mu'\\
&\quad+\frac{\mu_0}{2}\int_{0}^{1}P^{(0)}(\mu,\mu')R^{(0)}(n-1:\mu',\mu_0)d\mu'\\
&\quad+\frac{\mu\mu_0}{4}\sum_{n'=1}^{n-2}\int_{-1}^{0}\int_{0}^{1}R^{(0)}(n':\mu,\mu')P^{(0)}(\mu',\mu'')R^{(0)}(n-n'-1:\mu'',\mu_0)d\mu''d\mu',\\
&\qquad\qquad l=1,2,\cdots\quad n\geq 3
\end{aligned}
\tag{36}
$$

$$
\begin{aligned}
&(\mu+\mu_0)R_c^{(l)}(n:\mu,\mu_0)\\
&\quad=\frac{\mu}{2}\int_{-1}^{0}\left[R_c^{(l)}(n-1:\mu,\mu')P_c^{(l)}(\mu',\mu_0)-R_s^{(l)}(n-1:\mu,\mu')P_s^{(l)}(\mu',\mu_0)\right]d\mu'\\
&\quad+\frac{\mu_0}{2}\int_{0}^{1}\left[P_c^{(l)}(\mu,\mu')R_c^{(l)}(n-1:\mu',\mu_0)-P_s^{(l)}(\mu,\mu')R_s^{(l)}(n-1:\mu',\mu_0)\right]d\mu'\\
&\quad+\frac{\mu\mu_0}{4}\sum_{n'=1}^{n-2}\int_{-1}^{0}\int_{0}^{1}\Big[R_c^{(l)}(n':\mu,\mu')\Big\{P_c^{(l)}(\mu',\mu'')R_c^{(l)}(n-n'-1:\mu'',\mu_0)\\
&\qquad\qquad-P_s^{(l)}(\mu',\mu'')R_s^{(l)}(n-n'-1:\mu'',\mu_0)\Big\}\\
&\qquad\qquad-R_s^{(l)}(n':\mu,\mu')\Big\{P_s^{(l)}(\mu',\mu'')R_c^{(l)}(n-n'-1:\mu'',\mu_0)\\
&\qquad\qquad-P_c^{(l)}(\mu',\mu'')R_s^{(l)}(n-n'-1:\mu'',\mu_0)\Big\}\Big]d\mu''d\mu',\\
&\qquad\qquad l=1,2,\cdots\quad n\geq 3
\end{aligned}
\tag{37}
$$

AMTD
5, 881–907, 2012

$$
\begin{aligned}
&(\mu+\mu_0)R_s^{(l)}(n:\mu,\mu_0)\\
&\quad=\frac{\mu}{2}\int_{-1}^{0}\left[R_c^{(l)}(n-1:\mu,\mu')P_s^{(l)}(\mu',\mu_0)+R_s^{(l)}(n-1:\mu,\mu')P_c^{(l)}(\mu',\mu_0)\right]d\mu'\\
&\quad+\frac{\mu_0}{2}\int_{0}^{1}\left[P_c^{(l)}(\mu,\mu')R_s^{(l)}(n-1:\mu',\mu_0)+P_s^{(l)}(\mu,\mu')R_c^{(l)}(n-1:\mu',\mu_0)\right]d\mu'\\
&\quad+\frac{\mu\mu_0}{4}\sum_{n'=1}^{n-2}\int_{-1}^{0}\int_{0}^{1}\Big[R_c^{(l)}(n':\mu,\mu')\Big\{P_c^{(l)}(\mu',\mu'')R_s^{(l)}(n-n'-1:\mu'',\mu_0)\\
&\qquad\qquad+P_s^{(l)}(\mu',\mu'')R_c^{(l)}(n-n'-1:\mu'',\mu_0)\Big\}\\
&\qquad+R_s^{(l)}(n':\mu,\mu')\Big\{P_c^{(l)}(\mu',\mu'')R_c^{(l)}(n-n'-1:\mu'',\mu_0)\\
&\qquad\qquad+P_s^{(l)}(\mu',\mu'')R_s^{(l)}(n-n'-1:\mu'',\mu_0)\Big\}\Big]d\mu''d\mu'.\\
&\qquad\qquad l=1,2,\cdots\quad n\geq 3
\end{aligned}
\tag{38}
$$

3.3 Asymptotic form

In practice, the convergence of Eq. (26) is very slow when ϖ is very close to 1. In order to solve this problem, the asymptotic form of $R(n)$ is proposed for higher-order scattering (Uesugi et al., 1970, Mukai et al., 1979):

$$R(n:\Omega,\Omega_0)=A(\Omega,\Omega_0)n^{-3/2}\exp\left[-d(\Omega,\Omega_0)/n\right]$$

$$\cong A(\Omega,\Omega_0)\,n^{-3/2}\left[1-d(\Omega,\Omega_0)/n+\mathrm{O}(n^{-2})\right] \tag{39}$$

where the values of $A(\Omega,\Omega_0)$ and $d(\Omega,\Omega_0)$ are successively calculated, and they converge for large $n^* >> 1$

$$A(\Omega,\Omega_0)=R(n^*:\Omega,\Omega_0)n^{*3/2}\exp\left[-d(\Omega,\Omega_0)/n^*\right] \tag{40}$$

AMTD
5, 881–907, 2012

Employing of Eq. (39) for the total reflection function for $n > n^* >> 1$ means that Eq. (10) becomes

$$R(\Omega,\Omega_0) = \sum_{n=1}^{n=n*} \varpi^n R(n:\Omega,\Omega_0) + A(\Omega,\Omega_0) \sum_{n=n*+1}^{\infty} \varpi^n n^{-3/2} \exp\left[-d(\Omega,\Omega_0)/n\right]. \tag{41}$$

The second term of Eq. (41) can be rapidly calculated by using the following transformation from summation to integration putting $a = -\ln\varpi$:

$$\sum_{n=n*+1}^{n=\infty} \varpi^n n^{-3/2} \exp\left[-d(\Omega,\Omega_0)/n\right] \cong \int_{n*}^{\infty} x^{-3/2} e^{-ax} dx - d(\Omega,\Omega_0) \int_{n*}^{\infty} x^{-5/2} e^{-ax} dx. \tag{42}$$

It is noted that the above approximation produces the error in numerical calculationsugnyway, through integrating of Eq. (42), Eq. (41) can be written as

$$\begin{aligned} R(\Omega,\Omega_0) = {} & \sum_{n=1}^{n=n*} \varpi^n R(n:\Omega,\Omega_0) + 2A n^{*-1/2}[e^{-an*} - (\pi a n^*)^{1/2} erfc(\sqrt{a n^*})] \\ & - \tfrac{2}{3} A d\, n^{*-3/2}[(1-2a\, n*)e^{-an*} + 2\sqrt{\pi}(a n^*)^{3/2} erfc(\sqrt{a n^*})], \end{aligned} \tag{43}$$

where *erfc* represents the complementary error function. The accuracy of the asymptotic form of Eq. (43) has been checked for the conservative case (i.e. ϖ=1) by using the flux conservation law.

$$1 = \frac{1}{\pi} \int R(\Omega,\Omega_0) \mu\, d\Omega \tag{44}$$

Certainly Eq. (43) allowed us to compute the total reflection function by using low-order scattering alone, but n* was necessary to be greater than 30 in order to depress the relative errors to be less than 0.1 % for our numerical calculations in the strongly anisotropic scattering cases. That is to say, the convergence of Eq. (10) is not so improved by employing the asymptotic form of Eq. (43). With respect to the convergence of successive order of scattering, it is well known that the values of albedo for single

AMTD
5, 881–907, 2012

scattering play the sufficient role. In such a case that the values of albedo for single scattering are less than unity (i.e. $\varpi < 1$), the convergence of Eq. (10) could be reasonably rapid (Mukai et al., 1979). In usual, however, we do not have high absorption of aerosols except fires (Mishchenko et al., 1999).

4 Retrieved results for Aerosol events

Our new computation code for implementing the method of successive order of scattering (MSOS) was applied to the Earth-observing Aqua/MODIS sensor (King et al., 1992) data in order to retrieve the characteristics of biomass burning aerosols. Because the MSOS is efficiently useful for the absorbing aerosols as mentioned in the previous session. Figure 2 presents a colour composite image as ([r : g : b]=[0.65 µm, 0.55 µm, 0.46 µm]) with Aqua/MODIS data over the boundary region between Brazil and Bolivia in the south America on 21 in September of 2005. Each center of each square denoted by blue (S1) and yellow (S2) is represented by the position of (12° S, 64° W) in Brazil and (14° S, 63° W) in Bolivia, respectively, which are concerne3d hereafter and the points A and B denote AERONET sites of Alta Floresta (9° S, 56° W) and Rio Branco (9° S, 67° W), respectively. The AERONET program involves worldwide ground-based sun photometric observation networks run by NASA. These provide spectral information about the aerosol optical thickness (AOT) and the Ångström exponent (α). The data are processed and updated by the standard AERONET processing system. The system performs cloud screening, and the observational error is less than 0.01 in all wavelengths.

Omar et al. (2005) proposed using a clustering method for the automatic classification of aerosol observations into 6 categories (desert dust, biomass burning, background/rural, polluted continental, polluted marine and dirty pollution) according to their properties. They also confirmed the consistency and robustness of the method through a cross-validation check. The aerosol sizes in the aerosol model were assumed to follow a bimodal log-normal distribution, with r and σ denoting the mean and standard

AMTD
5, 881–907, 2012

deviation of the geometric radii of the particles, respectively. That is to say the volume distribution function for each aerosol model is represented by the (r_f, σ_f and (r_c, σ_c variables represent the fine and coarse particles, respectively. In this study we used this work of Omar et al. but made the following simplifications, which are described in detail by Yokomae et al. (2011) and refer to Table 1. Firstly, we adopted a bimodal form for the volume distribution with the fine-mode particles constituting a fraction "f" of the total ones. Secondly, we adopted a determinant set as (r_f, $\sigma_f = (0.14, 1.86)$ and (r_c, σ_c) = (3.42, 2.34) averaging over each value of 6 aerosol categories proposed by Omar et al. (2005). Thus the volume distribution for aerosol sizes in the present model was assumed to follow the bimodal log-normal function given by

$$\frac{dV(r)}{d\ln r} = \frac{f}{\sqrt{2\pi}\ln\sigma_f}\exp\left[-\frac{(\ln r - \ln r_f)^2}{2\ln^2\sigma_f}\right] + \frac{(1-f)}{\sqrt{2\pi}\ln\sigma_c}\exp\left[-\frac{(\ln r - \ln r_c)^2}{2\ln^2\sigma_c}\right], \tag{45}$$

where the parameter f represents the ratio of fine particles to total particles.

Then the above mentioned parameter f and the complex refractive indices of biomass aerosols $m(\lambda) = n(\lambda) - k(\lambda)i$ were the required values. This study employed the complex refractive indices for dust aerosol models listed in Table 2, where A, B and C represent the values retrieved from ground measurements at the AERONET sites of Alta Floresta, Rio Branco in Brazil and d'Almeida et al. (1991), respectively.

Our retrieval process of biomass burning aerosols from the forest fire is based on comparison between satellite data and the reflectance calculated using a semi-infinite model. The thick and thin solid curves in Fig. 3 present the simulated values of the reflectance ($R(\lambda)$) for aerosol models with parameters (f) and refractive index (m) for case-A and case-B, respectively, for the concerned directional condition in a two-channel diagram at wavelengths of $\lambda = 0.46$ and 0.55gμm. The coloured dot symbols in Fig. 3 denote the satellite data within each square painted by the same colour in Fig. 2, i.e. blue and yellow represent the squares S1 and S2 in Fig. 2, observed on 21 September of 2005 by Aqua/MODIS. First it should be mentioned that the simulated results with the case-C refractive index are far away from the satellite data of S1 and

AMTD
5, 881–907, 2012

S2 in the two-channel diagram at wavelengths of $\lambda = 0.46$ and 0.55µm. Furthermore it is shown from Fig.3 that neither case-C nor case-B is good at to explain the satellite data of S1 and S2. And hence we can say that the possible candidates of refractive index of aerosol model to explain the satellite data of S1 and S2 exist around the case-A values.

Now we shall try to retrieve the refractive indices more precisely in the neighbourhood of case-A, i.e. m(0.46 µm) = 1.568 − 0.007018i and m(0.55 µm) = 1.586 − 0.006390i. Assuming the values of n(0.55 µm), k(0.55 µm) and n(0.46 µm) are fixed at the same values as those of case-A, the imaginary (k(0.46 µm)) part of refractive index at a wavelength of 0.46 µm is just a free parameter. When the 5 % of magnitude is fluctuated from the value of k(0.46 µm) in case-A, k(0.46 µm) = 0.00656 and 0.00732 provide us with the simulated values of reflectance denoted by the dashed (A-R1) and dot-dashed (A-R2) curves in Fig. 3, respectively. It is of interest to mention that the satellite data of S1 and S2 exist between these two curves as a result. Namely it can be concluded that the aerosol model for S1 and S2 data take the refractive index of case-A, although the imaginary part is slightly different at a wavelength of 0.46 µm.

As mentioned above fine-mode fraction "f" for a bimodal size distribution function by Eq. (45) indicates particle size, then roughly speaking S1 data show the rather larger aerosols than those suggested from S2 data. Anyway from Fig. 3, the parameter "f" suitable to the MODIS data S1 and S2 takes the values of $0.185 \leq f \leq 0.31$. For reference, size distribution functions with $f = 0.185$ and 0.31 is denoted by the red curves in Fig. 4, where the black solid curves show typical size distribution functions for polluted marine aerosol type and biomass burning one classified by Omar et al. (2005). It is possible to say that our retrieved aerosol size is reasonable to the atmospheric particles emitted after forest fire, because both curves in red and black in Fig. 4 coincide with each other.

Accordingly, based on our retrieval algorithm with the Aqua/MODIS data at wavelengths of 0.46 and 0.55 µm, it is possible to draw the conclusion that the aerosols for the biomass burning observed over the boundary region between Brazil and Bolivia on 21 in September of 2005 contained rather large particles with $f \sim 0.25[0.185, 0.31]$ and the values of the refractive indices (m) retrieved from the ground measurements at AERONET/Alta Floresta sites in Brazil.

5 Conclusions

It is found that dense aerosol events can be well simulated by a semi-infinite radiative-transfer model. New algorithms for aerosol retrieval based on the proposed aerosol models and the semi-infinite radiative-transfer simulation code named MSOS (Method of Successive Order of Scattering) can be applied to the biomass burning aerosol events using Aqua/MODIS data. For a example, the dense-forest-fire can be deduced by a dense aerosol model with the size distribution function of $f \sim 0.25$ and the refractive index derived from AERONET data obtained at Alta Floresta site in Brazil based on a comparison of the simulation of MSOS and the MODIS data observed on 21 in September of 2005 over the boundary region between Brazil and Bolivia in the south America.

It has been shown in Mukai et al. (2011) that the aerosol properties for yellow dust storm retrieved from Aqua/MODIS data and our MSOS code coincide with the results of a numerical simulation with the SPRINTARS model and the ground measurements.

Acknowledgements. The authors thank NASA for distributing the MODIS data and the AERONET team for data processing. This work was supported in part by a Grant-in-Aid for Scientific Research from the Japan Society for the Promotion of Science (no. 23120708) and by Global Change Observation Mission—Climate (GCOM-C) by JAXA (no. JX-PSPC-308878). The work of A. Kokhanovsky was supported by the ESA Project CCi-aerosol.

References

d'Almeida, G. A., Koepke, P., and Shettle, E. P.: Atmospheric aerosols: global climatology and radiative characteristics, A. Deepak Publishing, Hampton, Virginia, USA, 1991.

Busbridge, I. W.: The mathematics of radiative transfer, Cambridge, 1960.
Chandrasekhar, S.: Radiative transfer, Dover publications, inc., New York, 1960.
Dubovik, O., Holben, B. N., Eck, T. F., Smirnov, A., Kaufman, Y. J., King, M. D., Tanré, D., and Slutsker, I.: Variability of absorption and optical properties of key aerosol types observed in worldwide locations, J. Atmos. Sci., 59, 590–608, 2002.
Hansen, J. E. and Travis, L. D.: Light scattering in planetary atmospheres, Space Science Reviews, 16, 527–610, 1974.
Holben, B. N., Eck, T. F., Slutsker, I., Tanré, D., Buis, J. P., Setzer, A., Vermote, E., Reagan, J. A., Kaufman, Y. J., Nakajima, T., Lavenu, F., Jankowiak, I., and Smirnov, A.: AERONET – A federated instrument network and data archive for aerosol characterization, Remote Sens. Environ., 66, 1–16, 1998.
Hulst, van de H.C.: The atmosphere of the Earth and planets, (edited by: G. P. Kuiper), Chicago Univ. Press, Chicago, 1949.
Hulst, van de H.C.: A new look at multiple scattering, NASA Institute for Space Studies, New York, 1963.
Hulst, van de H. C.: Multiple light scattering, vols. 1 and 2, Academic, New York, 1980.
King, M. D., Kaufman, Y. J., Menzel, W. P., and Tanré, D.: Remote sensing of cloud, aerosol, and water vapor properties from the Moderate Resolution Imaging Spectrometer (MODIS), IEEE Trans. Geosci. Remote Sens., 30, 2–27, 1992.
Kneizys, F. X., Shettle, E. P., Abreu, L. W., Chetwynd, J. H., Anderson, G. P., Gallery, W. O., Selby, J. E. A., and Clough, S. A.: Users guide to LOWTRAN 7, AFGL-TR-88-0177, Air Force Geophysics Laboratory, Hanscom AFB. MA., 1989.
Kokhanovsky, A. A.: Statistical properties of a photon gas in random media, Physical Review, 66, 036701-1-4, 2002.
Mishchenko, M. M., Dlugach, J. M., Yanovitskij, E. G., and Zakharova, N. T.: Bidirectional reflectance of flat, optically thick particulate layers: an efficient radiative transfer solution and applications to snow and soil surfaces, J. Quant. Spectrosc. Ra., 63, 409–432, 1999.
Mukai, S. and Mukai, T.: Interpretation of the Infrared Polarization of Venus, ICARUS, 38, 90–99, 1979.
Mukai, S. : Atmospheric correction of remote sensing images of the ocean based on multiple scattering calculations, IEEE T. Geosci. Remote Sens., 28, 696–702, 1990.
Mukai, S., Yokomae, T., Sano, I., and Nakata, M. : Aerosol retrieval for dense dust storms based on radiative-transfer simulations, J. Appl. Remote Sens., submitted, 2011.

Discussion Paper | Discussion Paper | Discussion Paper | Discussion Paper |

AMTD
5, 881–907, 2012

Multiple scattering in a dense aerosol atmosphere

S. Mukai et al.

Mukai(Nakata), M. and Nakajima, T.: A study of long-term trends in mineral dust aerosol distributions in Asia using a general circulation model, J. Geophys. Res., 109(D19204), doi:10.1029/2003JD004270, 2004.

Nakajima, T. and Tanaka, M.: Matrix formulations for the transfer of solar radiation in a plane-parallel scattering atmosphere, J. Quant. Spectrosc. Ra., 35, 13–21, 1986.

Omar, A. H., Won, J.-G., Winker, D. M., Yoon, S.-C., Dubovik, O., and McCormick, M. P.: Development of global aerosol models using cluster analysis of Aerosol Robotic Network (AERONET) measurements, J. Geophys. Res., 110, D10S14, 1–14, 2005.

Sano, I., Mukai, S., Okada, Y., Holben, B., Ohta, S., and Takamura, T.: Optical properties of aerosols during APEX and ACE-Asia experiments, J. Geophys Res., 108, 8649, doi:10.1029/2002JD003263, 2003.

Sobolev, V. V.: A treatise on radiative transfer, (translated by S. I .Gaposchkin), van Nostlsnd, Princeton, NJ, 1963.

Uesugi, A. and Irvine, W. M.: Multiple scattering in a plane-parallel atmosphere I. Successive scattering in a semi-infinite medium, The Astrophysical Journal, 159, 127–135, 1970.

Yokomae, T., Nakata, M., Sano, I., and Mukai, S.: Size distribution model for aerosols, NAIS Journal, in press, 2011.

Table 1. Size distribution parameters of each aerosol category from AERONET data (ref. Omar et al., 2005).

category	aerosol type	fine		coarse	
		r_m	σ	r_m	σ
1	desert dust	0.117	1.482	2.834	1.908
2	biomass burning	0.144	1.562	3.733	2.144
3	background/rural	0.133	1.502	3.590	2.104
4	polluted continental	0.158	1.526	3.547	2.065
5	polluted marine	0.165	1.611	3.268	1.995
6	dirty pollution	0.140	1.540	3.556	2.134
approximate form		**0.143**	**1.861**	**3.421**	**2.339**

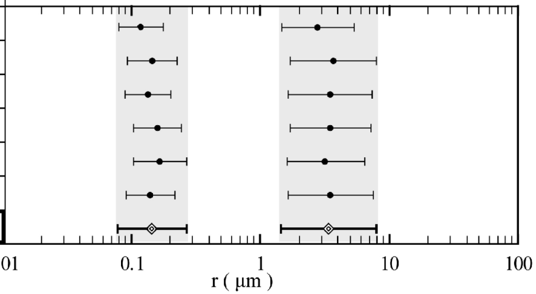

AMTD
5, 881–907, 2012

Multiple scattering in a dense aerosol atmosphere

S. Mukai et al.

Table 2. Refractive index of aerosol derived from AERONET (case-A and case-B) and d'Almeida et al. (1991) (case-C).

wavelength(µm)	case-A	case-B	case-C
0.460	1.568–0.007018*i*	1.541–0.014360*i*	1.750–0.4544*i*
0.550	1.586-0.006390*i*	1.544-0.012371*i*	1.750-0.4400*i*

AMTD
5, 881–907, 2012

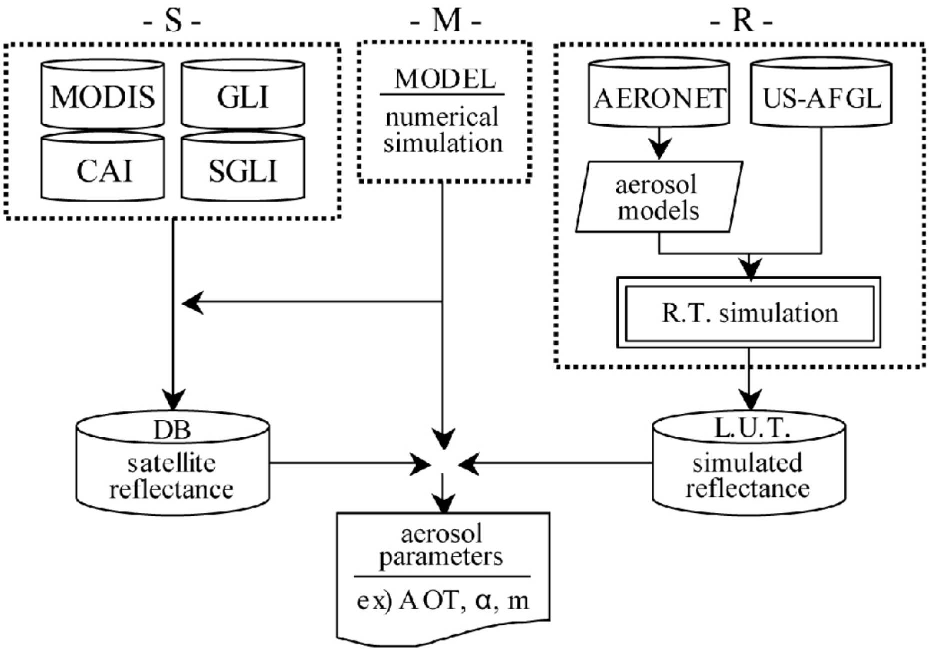

Fig. 1. A block diagram for satellite-based aerosol retrieval.

AMTD
5, 881–907, 2012

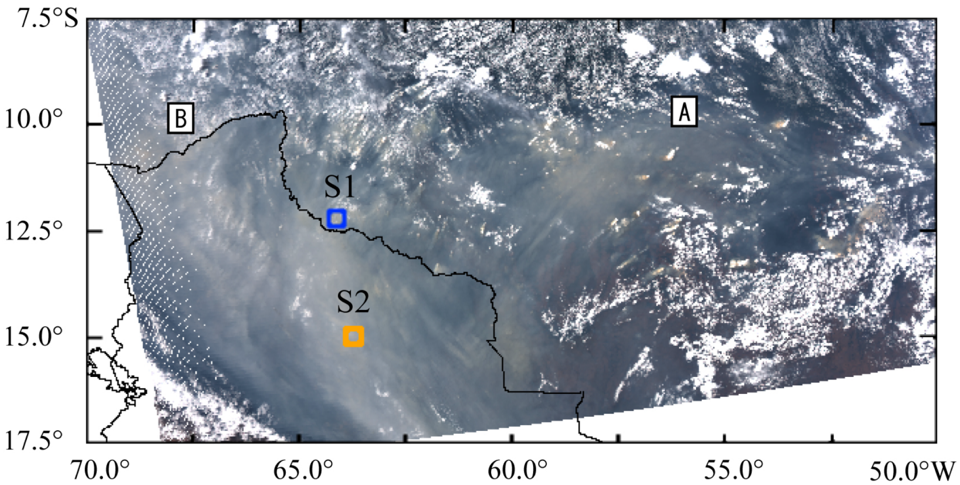

Fig. 2. A color composite image of biomass burning event from Aqua/MODIS data over the boundary region between Brazil and Bolivia on 21 in September of 2005. The points A and B denote AERONET sites of Alta Floresta in Brazil and Rio Branco in Bolivia, respectively.

AMTD
5, 881–907, 2012

Title Page
Abstract
Introduction
Conclusions
References
Tables
Figures
Back
Close
Full Screen / Esc
Printer-friendly Version
Interactive Discussion

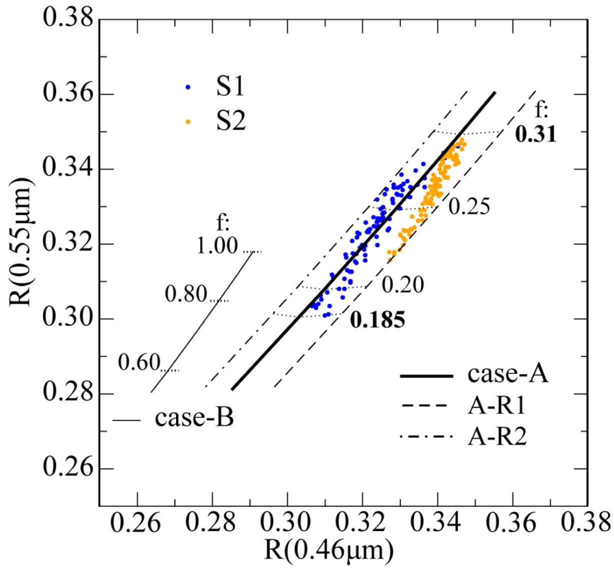

Fig. 3. Simulated values of the reflectance [R(λp] for aerosol models with size parameter (f) and the refractive indices (m) (refer to Table 2) in a two-channel diagram at wavelengths of 0.46 and 0.55 µm. The blue and yellow dot symbols denote the satellite data S1 and S2 in Fig. 2, respectively, observed on 21 September of 2005 by Aqua/MODIS.

AMTD
5, 881–907, 2012

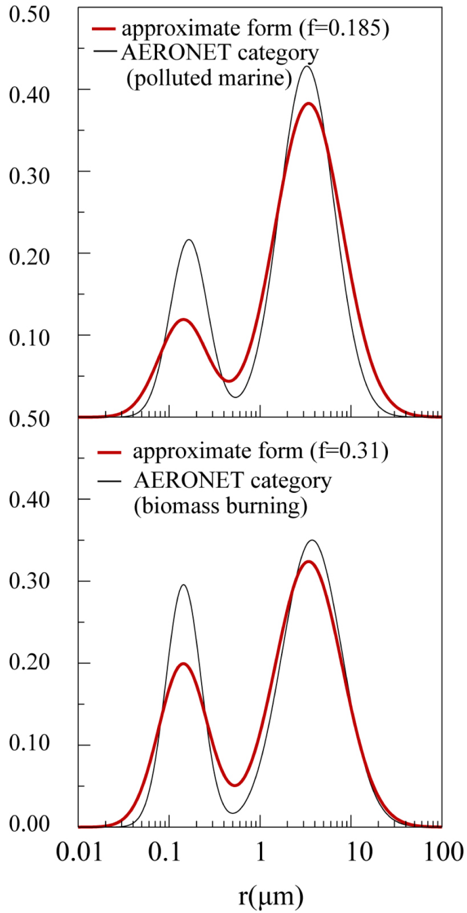

Fig. 4. Size distribution functions for AERONET category and approximate form defined by parameter "f" given by Eq. (45) are denoted by black curve and red one, respectively.